Use of impervious surface in urban land-use classification

Article *in* Remote Sensing of Environment · May 2006

DOI: 10.1016/j.rse.2006.02.010

2 authors:

Dengsheng Lu
Michigan State University
99 PUBLICATIONS **6,070** CITATIONS
SEE PROFILE

Qihao Weng
Indiana State University
142 PUBLICATIONS **6,472** CITATIONS
SEE PROFILE

Available online at www.sciencedirect.com
SCIENCE DIRECT
Remote Sensing of Environment 102 (2006) 146–160
Remote Sensing of Environment
www.elsevier.com/locate/rse

Use of impervious surface in urban land-use classification

Dengsheng Lu [a,*], Qihao Weng [b,1]

[a] Center for the Study of Institutions, Population, and Environmental Change, Indiana University, Bloomington, IN 47408, USA
[b] Department of Geography, Geology, and Anthropology, Indiana State University, Terre Haute, IN 47809, USA

Received 20 June 2005; received in revised form 8 February 2006; accepted 9 February 2006

Abstract

Impervious surface has been recognized as a key indicator in assessing urban environments. However, accurate impervious surface extraction is still a challenge. Effectiveness of impervious surface in urban land-use classification has not been well addressed. This paper explored extraction of impervious surface information from Landsat Enhanced Thematic Mapper data based on the integration of fraction images from linear spectral mixture analysis and land surface temperature. A new approach for urban land-use classification, based on the combined use of impervious surface and population density, was developed. Five urban land-use classes (i.e., low-, medium-, high-, and very-high-intensity residential areas, and commercial/industrial/transportation uses) were developed in the city of Indianapolis, Indiana, USA. Results showed that the integration of fraction images and surface temperature provided substantially improved impervious surface image. Accuracy assessment indicated that the root-mean-square error and system error yielded 9.22% and 5.68%, respectively, for the impervious surface image. The overall classification accuracy of 83.78% for five urban land-use classes was obtained.

Keywords: Impervious surface; Urban land-use classification; Linear spectral mixture analysis; Land surface temperature; Population density

1. Introduction

Improving urban land-use/cover classification accuracy has been an important issue in remote-sensing literature. Different approaches have been applied, which include incorporation of geographic data (Harris & Ventura, 1995), census data (Mesev, 1998), texture features (Lu & Weng, 2005; Myint, 2001; Shaban & Dikshit, 2001), and structure or contextual information (Gong & Howarth, 1990; Stuckens et al., 2000) into remote sensing spectral data. Moreover, expert systems (Hung & Ridd, 2002; Stefanov et al., 2001), fuzzy classification (Zhang & Foody, 2001), and merged multisensor data such as those between radar and Thematic Mapper (TM) data (Haack et al., 2002), and between SPOT and TM data (Gluch, 2002) have been applied. Much attention has recently been shifted to the development of more advanced classification algorithms, including neural network, contextual, object-oriented, and knowledge-based classification approaches (Stuckens et al., 2000; Thomas et al., 2003; Zhang & Foody, 2001; Zhang & Wang, 2003). However, urban land-use/cover classification is still a challenge with medium or coarse spatial resolution remotely sensed data due to the large number of mixed pixels and the spectral confusions among different land-use/cover types.

Mixed pixels have been recognized as a problem affecting the effective use of remotely sensed data in urban land-use/cover classification (Cracknell, 1998; Fisher, 1997). Traditional per-pixel classifiers, such as maximum-likelihood classifier, cannot effectively handle complex urban landscapes and the mixed-pixel problem. One of the recent major advances in urban land-use/cover analysis is Ridd's (1995) vegetation–impervious surface–soil (V–I–S) model. This model assumes that the spectral signature of land cover in urban environments is a linear combination of three components, namely vegetation, impervious surface, and soil. The V–I–S model has demonstrated to be an effective approach to cope with the mixed-pixel problem and provides a guideline for decomposing low-resolution images of urban landscapes and a link for these components to spectral signatures.

* Corresponding author. Tel.: +1 812 856 3102; fax: +1 812 855 2634.
E-mail addresses: dlu@indiana.edu (D. Lu), geweng@isugw.indstate.edu (Q. Weng).
[1] Tel.: +1 812 237 2255; fax: +1 812 237 8029.

0034-4257/$ - see front matter © 2006 Elsevier Inc. All rights reserved.
doi:10.1016/j.rse.2006.02.010

The conceptual V–I–S model may be implemented by using the technique of linear spectral mixture analysis (LSMA), which decomposes the spectral reflectance of a pixel into different proportions. LSMA is regarded as a physically based image-processing tool that supports repeatable and accurate extraction of quantitative subpixel information (Smith et al., 1990). Because of its effectiveness in handling the spectral mixture problem, LSMA has been widely used in many fields, such as mapping of land-cover types (Adams et al., 1995; Aguiar et al., 1999; Cochrane & Souza, 1998; DeFries et al., 2000; Lu et al., 2003). In urban studies, LSMA has shown the potential for estimating impervious surface and vegetation abundance and improving urban classification (Lu & Weng, 2004; Phinn et al., 2002; Rashed et al., 2001; Small, 2001, 2002; Wu & Murray, 2003). Because impervious surface is closely related to urban land-use patterns, the use of impervious surface may provide new insights for urban land-use classification.

Impervious surfaces are anthropogenic features through which water cannot infiltrate the soil, including roads, driveways, sidewalks, parking lots, rooftops, and so on. Research on impervious surface extraction from remotely sensed data has attracted interest since the 1970s. Slonecker et al. (2001) grouped methods of impervious surface extraction from remotely sensed data into three categories: interpretive applications, spectral applications, and modeling applications, which were mainly based on the achievements in the 1970s and 1980s. Brabec et al. (2002) summarized four ways for evaluating impervious surface: using a planimeter to measure impervious surface areas on an aerial photograph, counting the number of intersections on the overlaid grid on an aerial photograph, conducting image classification, and estimating impervious surface through the percentage of urbanization in a region. Recently, research in impervious surface extraction has moved toward per-pixel image classification (Dougherty et al., 2004; Hodgson et al., 2003; Jennings et al., 2004), subpixel classification (Civico et al., 2002; Ji & Jensen, 1999; Phinn et al., 2002; Rashed et al., 2003), and decision tree modeling (Goetz et al., 2004; Jantz et al., 2005; Yang et al., 2003a, 2003b). Extraction of impervious surfaces have also been conducted by the combination of high-albedo and low-albedo fraction images (Wu, 2004; Wu & Murray, 2003), and by establishing the relationship of impervious surfaces with vegetation cover (Bauer et al., 2004; Gillies et al., 2003).

Extraction of impervious surfaces is still a challenge because of the complexity of urban and suburban landscapes and the limitation of remotely sensed data in spectral and spatial resolutions. The extractions based on an image classification are often underestimated due to the heterogeneity of urban landscapes. The impervious surfaces may be mixed with other land cover types, such as trees, grasses, and soils. The difficulty in selecting training samples for impervious surfaces is a major factor resulting in land-use/cover misclassification. When high spatial resolution data, such as IKONOS, are used for impervious surface mapping (Goetz et al., 2003), shadows caused by tall buildings or large tree crowns may create a severe problem in effective extraction (Dare, 2005). Because of the high inverse correlation between vegetation cover and impervious surface areas in urban landscapes, one potential approach for impervious surface extraction is through the use of vegetation cover, such as tasseled cap greenness (Bauer et al., 2004) and fractional vegetation cover from the normalized difference vegetation index (Gillies et al., 2003). However, different seasons may result in large variations in impervious surface estimation. An alternative approach is to use the LSMA approach. Impervious surfaces may be directly extracted from multispectral images as one of the end members (Phinn et al., 2002; Rashed et al., 2001). The impervious surface estimation may be improved by the addition of low-albedo and high-albedo fraction images resulting from spectral mixture analysis (Wu, 2004; Wu & Murray, 2003). Because a low-albedo fraction image may relate to different kinds of features, including water, canopy shadows, building shadows, moisture in grass or crops, and dark impervious surface materials, it is critical to remove other types of covers from the low-albedo fraction image before it is used for the extraction of impervious surfaces. However, previous research has not examined the advantage of this approach. Because of different thermal responses between impervious surface and other cover types, the use of thermal infrared data may be able to aid impervious surface extraction. Schueler (1994) noted that impervious surface areas could yield temperature up to 10–12 degrees higher than the fields and forests they replaced, because impervious surfaces can hold and emit more heat than natural features. Since the usefulness of thermal infrared images, such as those from Landsat TM/ETM+ or Terra ASTER data, has not been examined for assisting impervious surface extraction, our objectives of this paper are to test the feasibility and effectiveness of using land surface temperature data to improve impervious surface mapping, and then to classify urban land-use classes based on the combined use of impervious surface and population density, because land-use distributions are closely related to both patterns of impervious surface and population density.

2. Study area and data used

2.1. Description of study area

Indianapolis/Marion County, Indiana, USA, was chosen as the study area (Fig. 1). It possesses several advantages that make it an appropriate choice for such a study. It has a single central city, and other large urban areas in the vicinity have not influenced its growth. The city is located on a flat plain and is relatively symmetrical, having possibilities of expansion in all directions. Like many other American cities, Indianapolis is rapidly increasing in population and in area. The areal expansion occurs through encroachment into the adjacent agricultural and non-urban land. Certain decision-making forces, such as density of population, distance to work, property value, and income structure, encourage some sectors of metropolitan Indianapolis to expand faster than others. Extracting information of impervious surface from satellite images

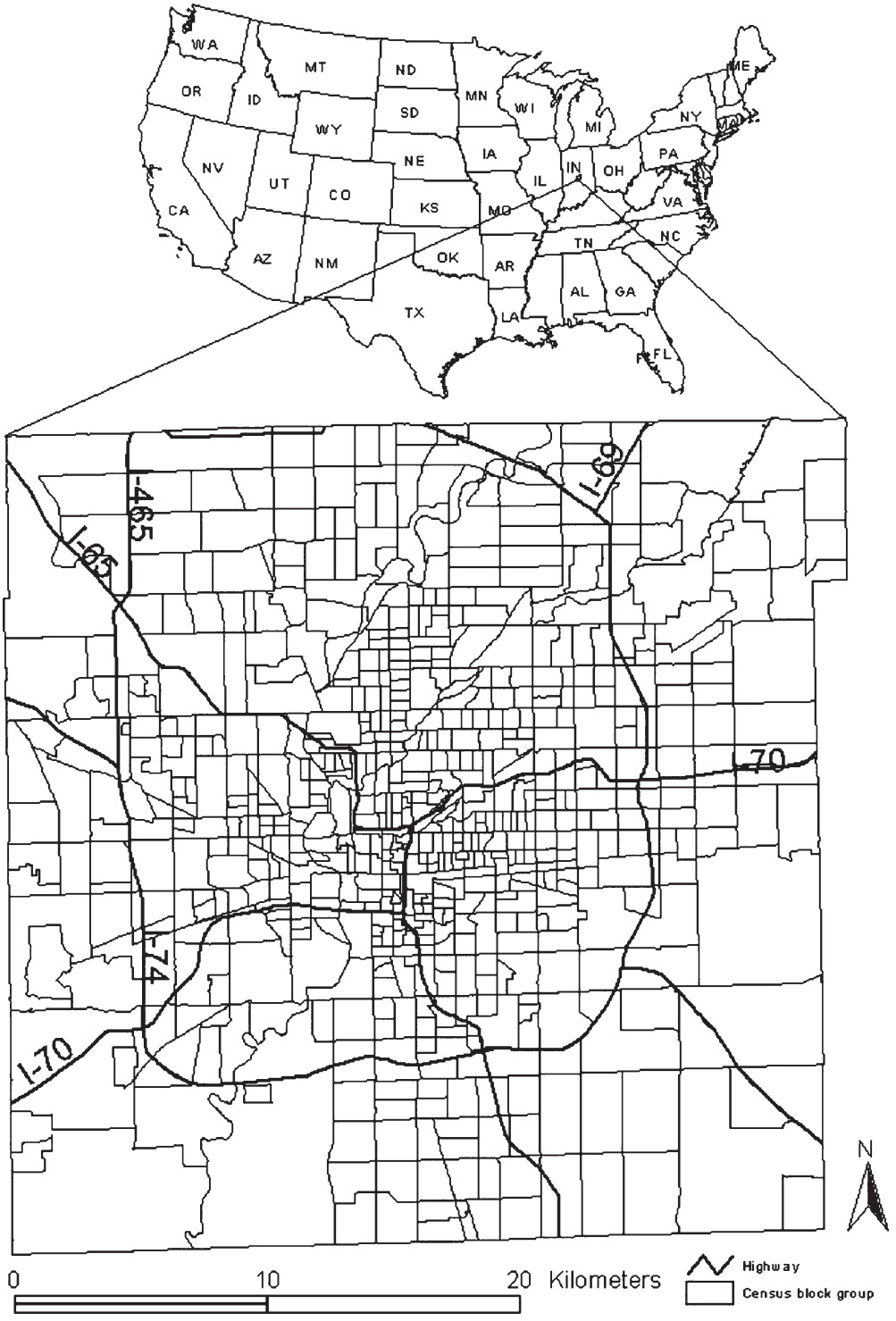

Fig. 1. Study area – Marion County (city of Indianapolis), Indiana, USA.

allows for monitoring urban changes over time, and integrating imperviousness into other spatial and non-spatial data for environmental management and urban planning activities.

2.2. Data sets

A Landsat 7 ETM+ image (path 21/row 32) of Marion County, Indiana, which was acquired on June 22, 2000 under clear weather conditions, was used in this research. The ETM+ image has one panchromatic band with 15-m spatial resolution, six reflective bands with 30-m spatial resolution, and one thermal infrared band with 60-m spatial resolution. The ETM+ data were geometrically rectified with 1:24,000 topographic maps. The root-mean-square error (RMSE) during image rectification was less than 0.2 pixels. A nearest-neighbor algorithm was used to resample the ETM+ image (including

the six reflective bands and the thermal infrared band) to a pixel size of 30 m × 30 m during image rectification. The ETM+ reflective bands were used to develop fraction images with LSMA, and the thermal infrared band was used to compute land surface temperature. The ETM+ panchromatic band was not used for the research described in this paper. No atmospheric calibration was conducted for the ETM+ image, because previous research had demonstrated that atmospheric calibration did not have an effect on fraction images when image end members were used (Lu et al., 2004; Small, 2004).

A land surface temperature image (Fig. 2) was directly used in this paper. A detailed description of the computation of land surface temperature from the ETM+ thermal infrared band was provided in Weng et al. (2004). The temperature gradually decreased from the highest values in commercial areas (such as A in Fig. 2), to medium values in high- and medium-intensity residential areas (such as B and C), to lowest values in non-urban areas such as crops, forested lands, and water (such as D, E, and F). The difference in land surface temperature between impervious surfaces and other cover types provided the potential to distinguish impervious surfaces from other cover types in the study area.

The 2000 census data in a shapefile format were used for assisting urban land-use classifications. Because of the difference in coordinate systems between census data and the ETM+ image, the geographic coordinate of the census data was converted into UTM to be consistent with the coordinate system of the ETM+ image. In the census data, population data were organized at three levels: tract, block group, and block. The block level provided the most detailed population information and was thus used in this research. Because the size of each block depended on the residential pattern, it was necessary to calculate population density (i.e., population/area at the block level, persons/km^2) in order to eliminate the impact of different block sizes. Fig. 3 illustrated population density distribution in the study area. The population density in commercial/industrial areas and in agricultural areas was very low. The population was mainly distributed in residential areas of different intensities.

Orthophotographs were used for validation of impervious surface estimation results and for accuracy assessment of the

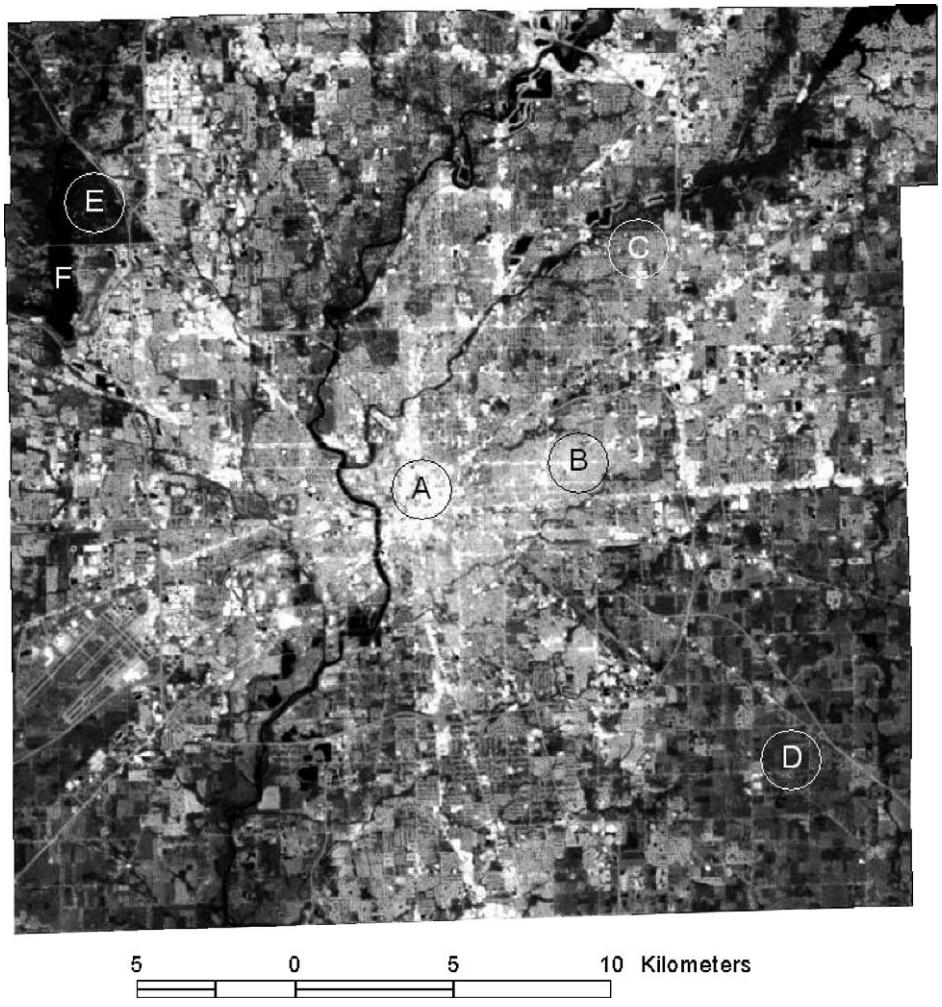

Fig. 2. Land surface temperature image derived from a Landsat 7 ETM+ thermal infrared band (land surface temperature ranges from 290 to 320 K, with lowest values in black and highest values in white): (A) commercial areas; (B) high-intensity residential areas; (C) medium-intensity residential areas; (D) agricultural lands; (E) forested lands; (F) water.

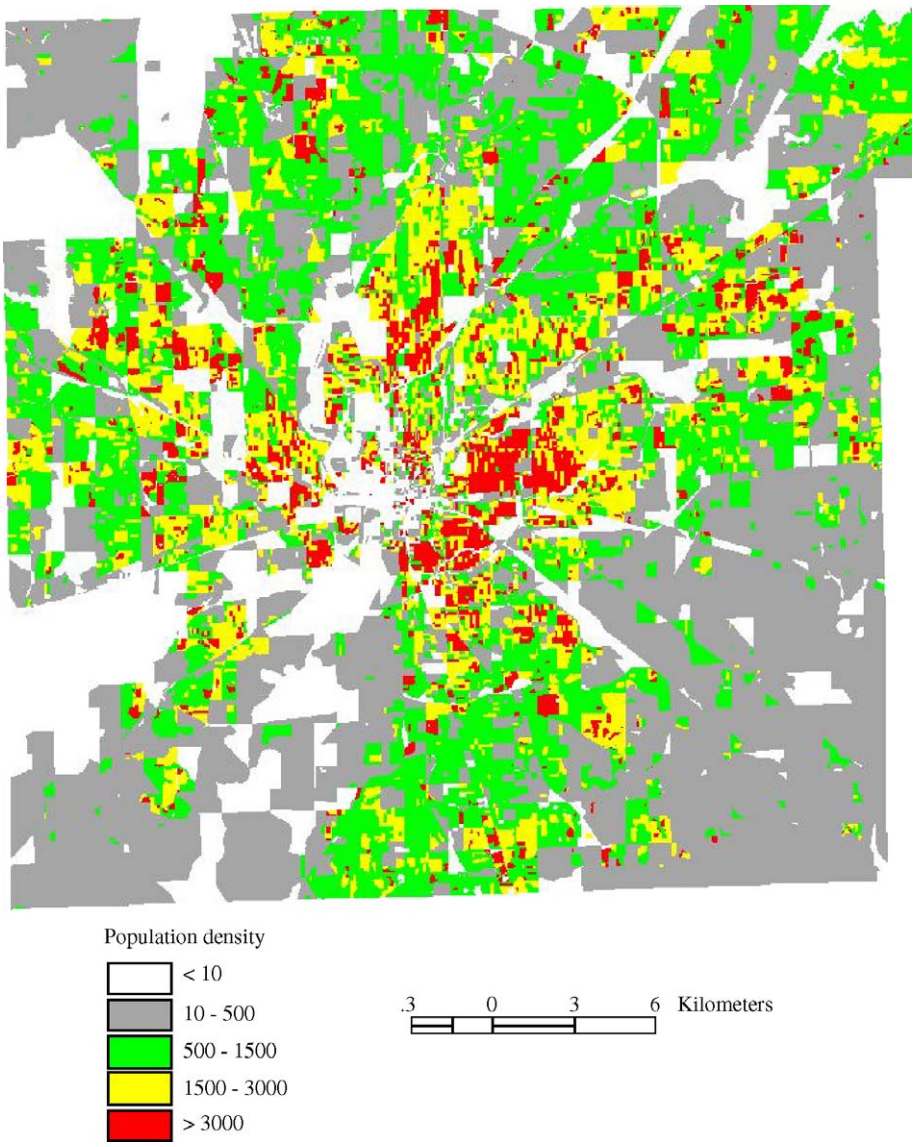

Fig. 3. A map of population density (persons/km^2) based on 2000 Census data.

urban land-use classification image. The color orthophotographs were provided by the Indianapolis Mapping and Geographic Infrastructure System, which was acquired in April 2003 for the entire county. The orthophotographs have a spatial resolution of 0.14 m. The coordinate system belongs to Indiana State Plane East, Zone 1301, with North American Datum of 1983. The orthophotographs were reprojected and resampled to 1-m pixel size for the sake of quicker display and shorter computing time.

3. Mapping of impervious surfaces

3.1. Linear spectral mixture analysis

The LSMA approach assumes that the spectrum measured by a sensor is a linear combination of the spectra of all components (end members) within the pixel and that the spectral proportions of the end members represent proportions of the area covered by distinct features on the ground (Adams et al., 1995; Mustard & Sunshine, 1999). In the LSMA approach, end member selection is a key step, and many approaches have been developed (Lu et al., 2003; Theseira et al., 2003). In practice, image-based end member selection methods are frequently used, because image end members can be easily obtained and they represent the spectra measured at the same scale as the image data. Image end members can be derived from the extremes of the image feature space, assuming that they represent the purest pixels in the images (Mustard & Sunshine, 1999). In order to effectively identify image end members and to achieve high-quality end members, different image transform approaches, such as principal component analysis and minimum noise fraction, may be used to transform the multispectral images into a new data set (Boardman & Kruse, 1994; Green et al., 1988). End members are then selected from the feature spaces of the transformed images (Cochrane & Souza, 1998; Garcia-Haro et

al., 1996; Small, 2001, 2002, 2004; Van der Meer & de Jong, 2000). In this research, image end members were selected from the feature spaces formed by the minimum noise fraction components.

3.2. Development of fraction images

The minimum noise fraction transform contains two steps: (1) de-correlation and rescaling of the noise in the data based on an estimated noise covariance matrix, producing transformed data in which the noise has unit variance and no band-to-band correlations; and (2) implementation of a standard principal component analysis of the noise-whitened data. The result of minimum noise fraction transform is a two-part data set, one part associated with large eigenvalues and coherent eigen-images, and a complementary part with near-unity eigenvalues and noise-dominated images (ENVI, 2000). In the minimum noise fraction transform, noise is separated from the data by using only the coherent portions, in order to improve spectral processing results.

In this research, the minimum noise fraction procedure was applied to transform the six ETM+ reflective bands into a new coordinate set. The first three components accounted for the majority of the information (approximately 99%) and were used for selection of end members. The scatterplots between minimum noise fraction components 1, 2, and 3 were illustrated in Fig. 4, showing the potential end members. Four end members: vegetation, high-albedo, low-albedo, and soil, were selected. A constrained least-squares solution was then applied to unmix the six ETM+ reflective bands into four fraction images, which were shown in Fig. 5. The high-albedo fraction image mainly related to impervious surface information in the urban area and some dry soils in agricultural areas. The commercial/industrial/transportation areas exhibited the highest values in the high-albedo fraction image. The value was gradually decreased from high-intensity residential to low-intensity residential areas. The low-albedo fraction image was more complex than other fraction images, because it contained different features, such as water, building shadows in the central business district, vegetation canopy shadows in forested areas,

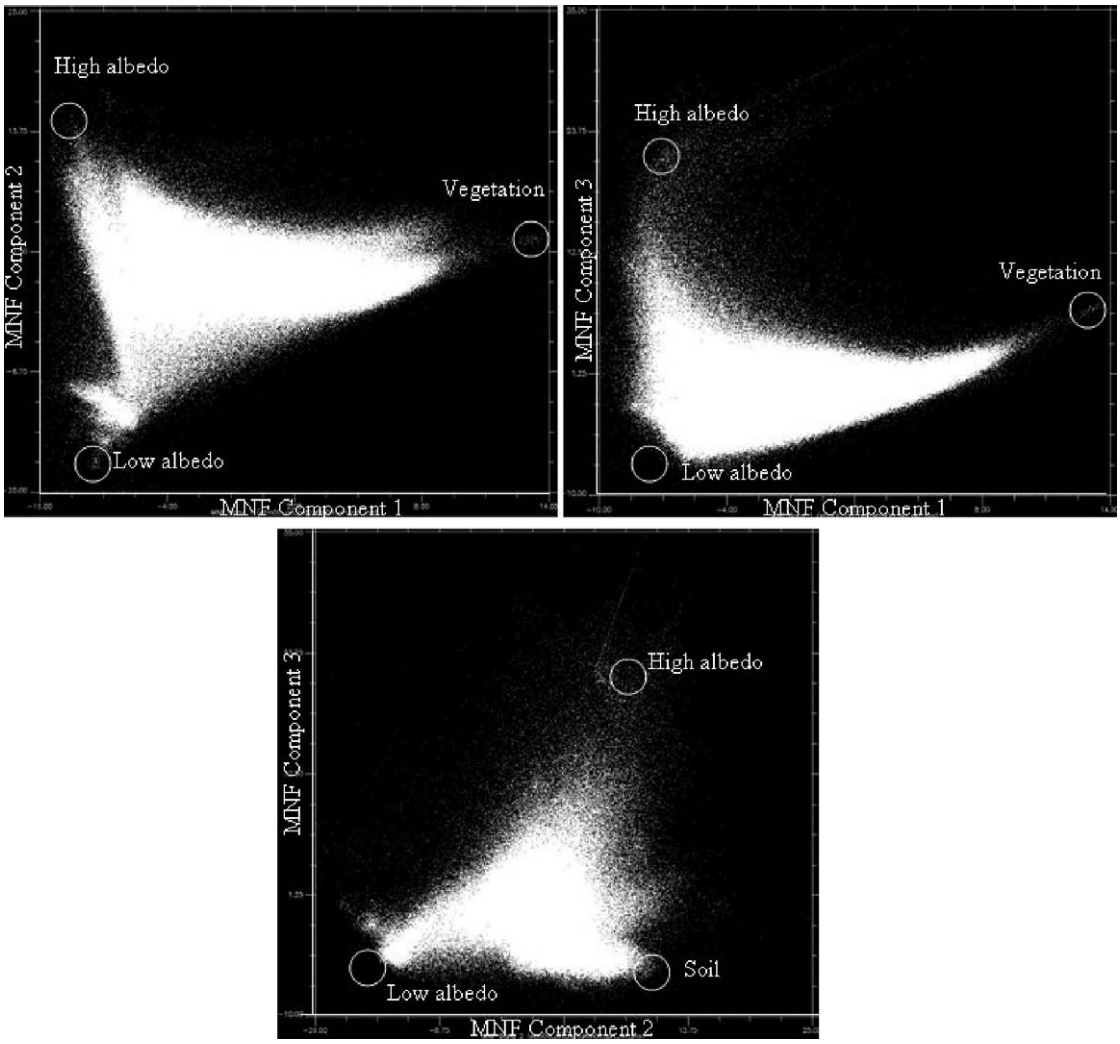

Fig. 4. Feature spaces between the three components from minimum noise fraction transform of the Landsat ETM+ image, illustrating four potential end members: high-albedo, low-albedo, vegetation, and soil.

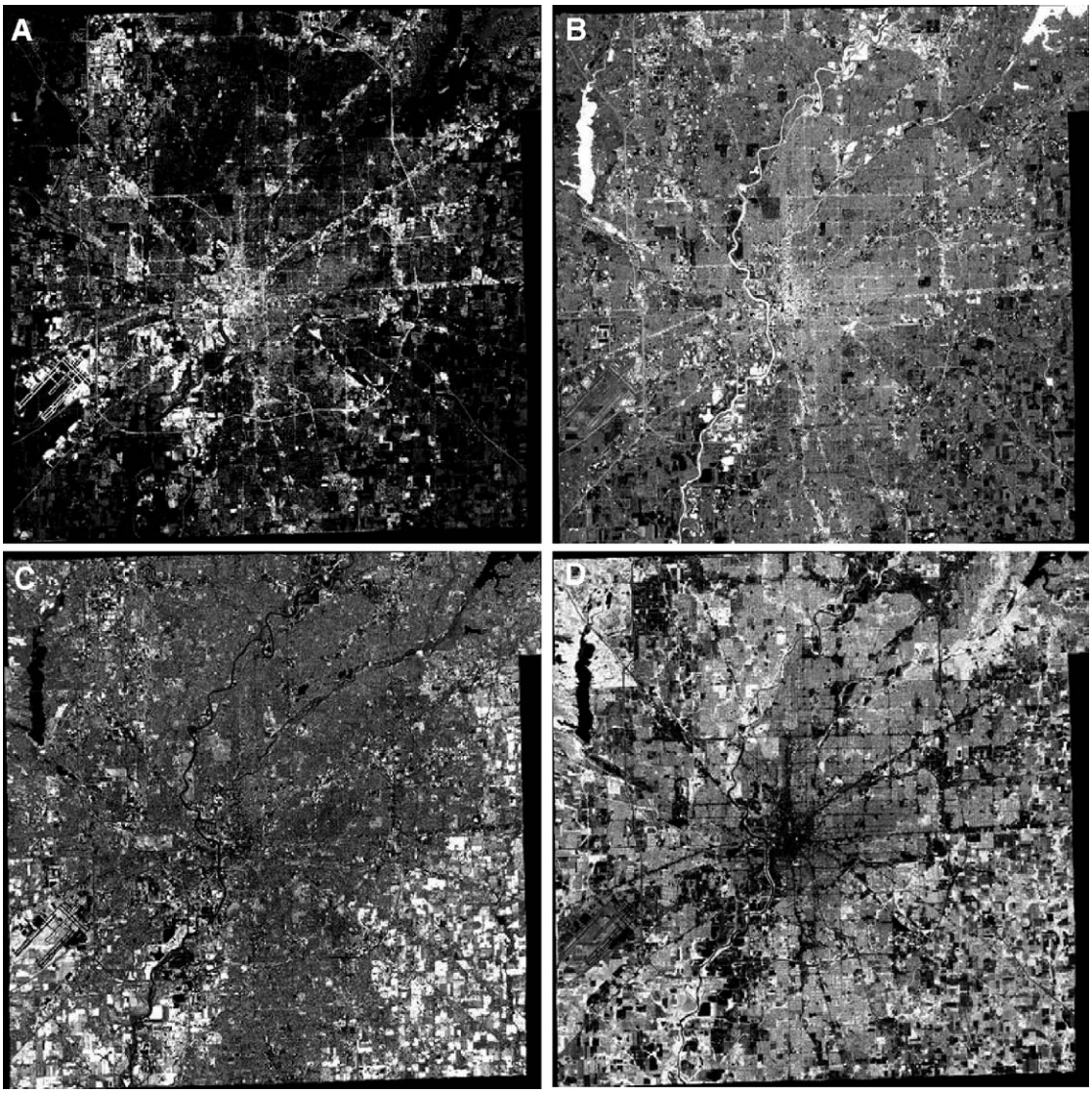

Fig. 5. Four fraction images from spectral mixture analysis of six ETM+ reflective bands (the fraction values range from 0 to 1, with lowest values in black and highest values in white in the fraction images): (A) high-albedo; (B) low-albedo; (C) soil; (D) vegetation.

and dark impervious surface materials. The soil fraction image highlighted the soil information located in the agricultural areas, and the vegetation fraction image detected high values in forest, pasture, grass, and croplands.

3.3. Development of impervious surface image

Extraction of impervious surface information from remotely sensed data is a complex procedure. As illustrated in Fig. 5, some other cover information was also included in the high-albedo and low-albedo fraction images. Direct extraction of impervious surface image through the addition of high-albedo and low-albedo fraction images is obviously unsuitable. Although the high-albedo fraction image related mainly to impervious surface information, such as buildings and roads, other cover type information, such as dry soils, was also included due to the similar spectral responses between some bright impervious surface materials and dry soils. On the other hand, the low-albedo fraction image highlighted information of water and shadows, such as water bodies, shadows from forest canopy and tall buildings, and moistures in crops or pastures. However, dark impervious surface information was also included in the low-albedo fraction image. It is important to develop a suitable approach for removal of other cover types from the low-albedo fraction image. This study found that the incorporation of land surface temperature provided a good premise to separate other cover types from impervious surface covers on the low-albedo fraction image.

The scatterplot between land surface temperature and low-albedo fraction images can reveal the different characteristics of land surface temperature and low-albedo fraction relationships among the land-use/cover classes (Fig. 6). The four corners A, B, C, and D represent four land covers: corner A represents grass/crops with very low values in both low-albedo fraction and land surface temperature images; corner B represents water with very high values in the low-albedo fraction image but very

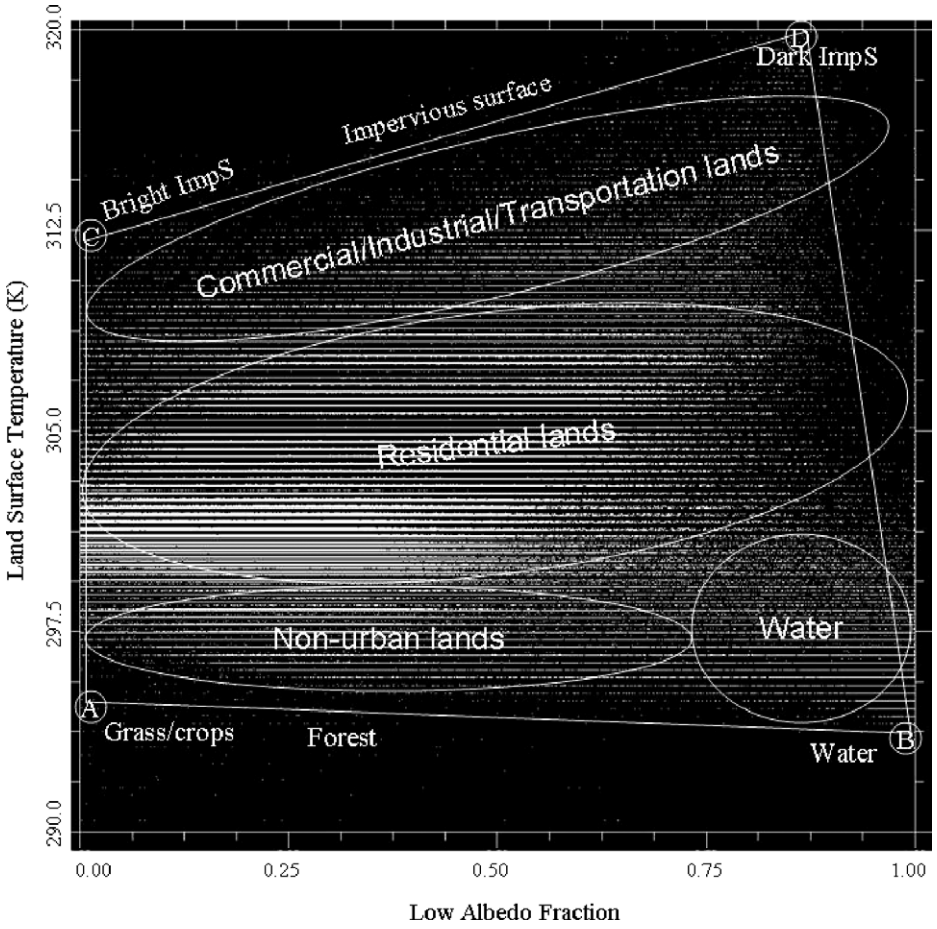

Fig. 6. Feature space created from the low-albedo fraction and land surface temperature images, illustrating the conceptual relationships of land-use/cover distribution.

low values in the land surface temperature image; corner C represents bright impervious surface objects with very low values in the low-albedo fraction image but very high values in the land surface temperature image; and corner D represents dark impervious surface objects with very high values in both the low-albedo fraction and land surface temperature images. Vegetation (crops, grass, and forest) and water possess lower land surface temperature values than built-up lands. Land surface temperatures of shadow areas are influenced strongly by the characteristics of the features generating the shadows and by their interactions with the surrounding pixels. For example, shadows in vegetation canopy were found to be generally cooler than shadows cast by tall buildings, because vegetation offsets absorptive heating by transpiration. For dark impervious surface objects with their absorptive features, land surface temperature increased as the values of low-albedo fraction increased. Shadow and moisture both generated a cooling effect, while impervious surface showed a heating effect.

For the high-albedo fraction image, impervious surface was predominantly confused with dry soils. So the soil fraction image may be used to remove the pixels of soils in the high-albedo fraction image. For the low-albedo fraction image, dark impervious surface was confused with water and shadows. Therefore, the critical process was to separate impervious surface from other cover type pixels, including water and vegetation (forest, pasture, grass, and crops). The following expert rules were used in this study:

(1) If the pixel values in the land surface temperature image were less than or equal to t_1, pixels in low-albedo and high-albedo fraction images would be assigned to zero, otherwise, pixel values in low-albedo and high-albedo fraction images would be kept; and
(2) If the pixel values in the soil fraction image were greater than t_2, pixels in high-albedo fraction image would be assigned to zero, otherwise, pixel values in the high-albedo fraction image would be kept.

In these rules, the t_1 and t_2 thresholds were identified based on reference data of water, vegetation, and soils. After other cover type pixels were removed from the low-albedo and high-albedo fraction images, the impervious surface image was then developed by addition of the modified low-albedo and high-albedo fraction images. Fig. 7 provided a comparison of the impervious surface images before and after the adjustment procedure. The final impervious surface image (B in Fig. 7) indicated that the other cover type information was successfully removed, comparing to the direct addition of low-albedo and high-albedo fraction

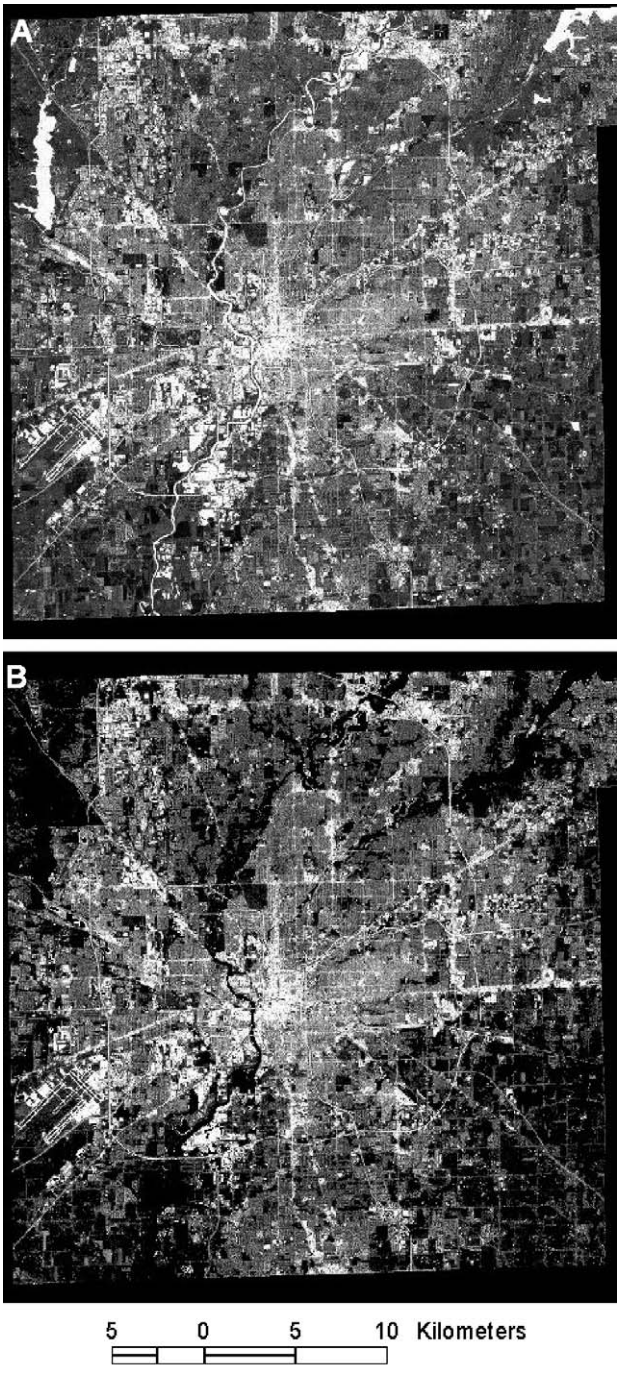

Fig. 7. Comparison of impervious surface images developed from different approaches (the image values range from 0 to 1, with lowest values in black and highest values in white): (A) based on the direct addition of high-albedo and low-albedo fraction images; (B) based on the addition of modified high-albedo and low-albedo fraction images, which other cover types were removed in the impervious surface image through the combinative use of land surface temperature and fraction images.

images (see A in Fig. 7). The gradient impervious surface change was obvious, from highest in commercial areas in the center of the study area, to medium in the high-intensity residential areas, to the lowest in the low-intensity residential areas.

3.4. Evaluation of impervious surface image

Accuracy assessment is an important step to ensure the quality of the impervious surface image. Selecting sufficient reference data through a suitable sampling scheme is important. Seventy-six sample plots with 10 × 10 pixel sizes (i.e., 300 m × 300 m) were initially selected on the impervious surface image. The plots were selected on the intersections between straight lines and cycles, with the distance of 100 pixels between two cycles (Fig. 8). The selected sample plots on the impervious surface image were linked to corresponding orthophotographs. The impervious surface objects within each sample plot were digitized on the orthophotograph. The proportion of impervious surface in each plot was then calculated. Because of the 3-year difference between ETM+ data (2000) and the referenced orthophotographs (2003), a careful check of each sample plot between a satellite color composite and orthophotographs was conducted. We found that seven sample plots showed apparent changes in landscape composition, and they were therefore removed during the accuracy assessment. Sixty-nine samples were finally used to assess the developed impervious surface image quality. The RMSE and system error were calculated (Wu, 2004). The accuracy assessment results were also analyzed with graphs (Fig. 9). The samples with low impervious surface (such as less than 0.6) tended to be overestimated, while samples with high impervious surface (such as greater than 0.6) were underestimated. The trend was in agreement with previous work, but the residuals were smaller than previous, similar work (Wu, 2004). The overall RMSE of 9.22% and a system error of 5.68% were obtained. For sample plots with less than 30% impervious surface, the RMSE was 9.98% and system error 8.59%. For sample plots with greater than or equal to 30% impervious surface, errors became smaller, with RMSE of 8.36% and system error of 2.77%.

4. Urban land-use classification

The classification approach used in this paper was based on the expert systems on the integration of impervious surface and population density data. Because of the unique feature of comparing with classifications based on spectral signatures, a suitable definition of land-use classes based on impervious surface and population density was required.

4.1. The classification scheme

Although medium spatial resolution data (10–100 m), such as Landsat TM/ETM+, were frequently used for land-cover classifications, the heterogeneity of urban environments and the large number of mixed pixels inherent images often induced difficulty in urban land-use/cover classification based on spectral signatures (Lu & Weng, 2004). Traditional per-pixel classification algorithms made it difficult to distinguish urban land-use/cover classes. Remote sensors mainly capture the features of Earth's surface, i.e., land-cover information. Hence, remotely sensed data are more suitable for land-cover classification, instead of land-use classification. In urban

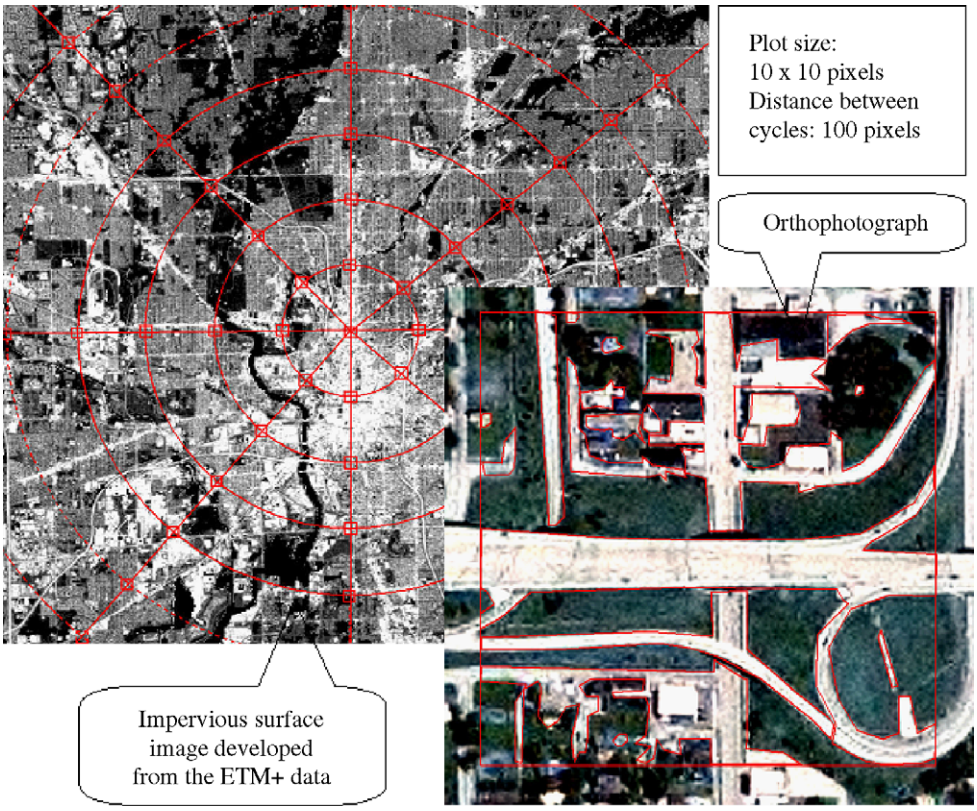

Fig. 8. Strategy for collection of reference data for the accuracy assessment of impervious surface image, illustrating the approach for allocating sample plots on the impervious surface image and for digitizing the impervious surface areas on the orthophotograph.

studies, however, land-use is more useful than land-cover information, because land-use is directly related to social–economic activities. A uniform definition of urban land-use classes is not available yet. Most previous research classified urban built-up areas into residential areas and commercial and industrial areas, or their subcategories when high-resolution data were used (Epstein et al., 2002; Phinn et al., 2002; Van der Sande et al., 2003; Zha et al., 2003). The criteria for classification of urban land-use/cover classes were different, and classification accuracies varied with the classification approaches employed and ancillary data incorporated (Phinn et al., 2002; Zha et al., 2003). Because of the close relationship between population density distribution and urban land-use pattern, our study classified the urban landscape into five land-use classes (i.e., very-high-, high-, medium-, and low-intensity residential lands, and commercial/industrial/transportation lands) based on the combination of impervious surface and population density images. Other classes included water and non-urban areas (vegetated and agricultural lands). Table 1 provides the definition of urban land-use types used in this paper.

4.2. Urban classification with integration of impervious surface and population density

The procedure of urban land-use classification based on the combination of impervious surface and population density images was illustrated in Fig. 10. The critical issue was to develop a high-quality impervious surface image and to establish expert rules of population density and impervious surface for each urban land-use class. In this research, five land-use classes were classified with a rule-based approach. Water and non-urban areas were classified based on low-albedo and high-albedo fraction images. The classification result from the 2000 ETM+ image (Fig. 11) demonstrated that the land-use seemed to display a concentric pattern from the center to the peripheral, transiting from commercial lands to very-high-, high-, medium-, and finally low-intensity residential lands. Commercial lands were mainly distributed in the center of the city. High- and very-high-intensity residential lands were distributed around commercial lands, especially in the eastern part of the city. Medium-intensity residential lands were located in the transition zone between high-intensity residential lands and non-urban areas. Low-intensity residential lands were scattered in the vegetated and agricultural areas.

4.3. Accuracy assessment of the land-use classification image

A common method for accuracy assessment of a classification image is through the use of an error matrix. Some important measures, such as overall accuracy, producer's accuracy, and user's accuracy, can be calculated form the error matrix (Congalton, 1991; Congalton & Green, 1999; Foody, 2002;

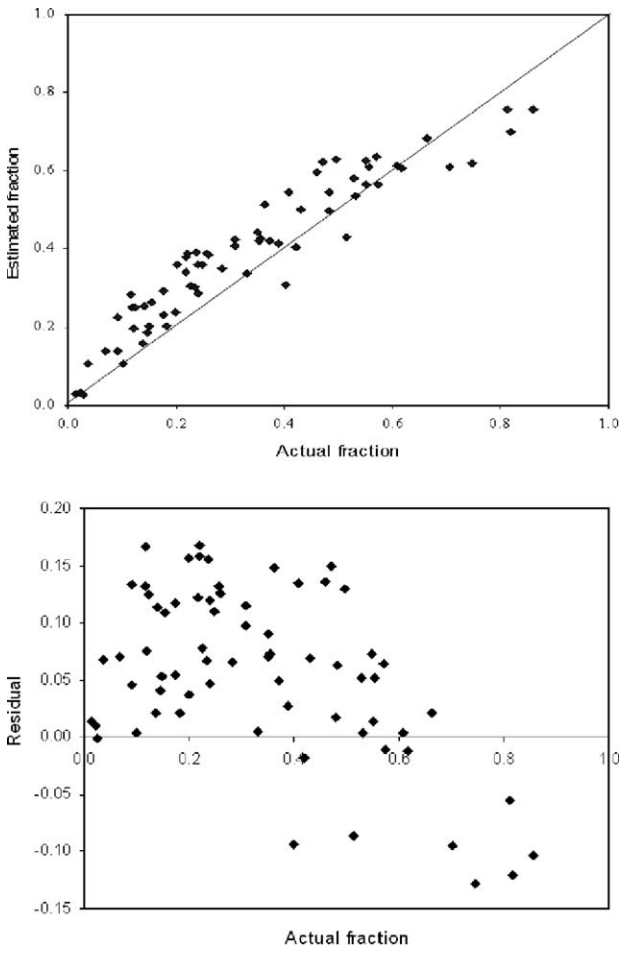

Fig. 9. Accuracy assessment results of estimated impervious surface from the Landsat ETM+ image.

Smits et al., 1999). In this study, a total of 230 sample plots were randomly allocated on the classified image. Excluding the plots outside the study area, 206 plots were examined on the high spatial resolution orthophotographs. Table 2 summarizes the accuracy assessment results. The overall classification accuracies of 87.38% for seven classes and of 83.78% for five urban land-use classes were achieved. The classification of commercial/industrial/transportation lands and medium-intensity residential lands were especially successful. The major errors were from the confusions between low-intensity residential lands and non-urban areas and between adjacent intensities of residential areas, such as low-intensity and medium-intensity residential lands.

5. Discussion

5.1. Issues related to estimation of impervious surface

This research showed that impervious surface was overestimated in the less-developed areas, but was underestimated in the well-developed areas. In the less-developed areas, such as medium- and low-intensity residential lands, impervious surfaces were often mixed with vegetation and soil. However, bright impervious surface objects had higher reflectance values than vegetation, especially in the visible and shortwave infrared bands, exaggerating their area proportions accounted for in the mixed pixels. Another factor was that dark impervious surface objects and water or shadows had similar spectral characteristics and similar values in the low-albedo fraction image. Dark impervious surfaces from the low-albedo fraction image may be over extracted based on the difference in land surface temperature because relative lower spatial resolution of Landsat ETM+ thermal band smoothed the boundaries between impervious surfaces and other cover types. In the well-developed areas, such as high-, and very-high-intensity residential lands, similar spectral responses in some bright impervious surfaces and dry soils created confusion, as shown in Fig. 5C. Tree crowns that cover portions of some impervious surfaces, such as roads, may be another reason resulting in underestimation of impervious surfaces.

Impervious surfaces are complex in terms of composition of materials. The limitation in spectral bands of medium spatial resolution images, such as Landsat TM/ETM+ data, and the high correlation among the image bands restrain the use of a large number of end members in the standard LSMA approach. Moreover, the image-based end member selection method may not effectively identify different impervious surface end members. However, some potential methods may remedy this problem. For example, hyperspectral imagery may be employed to extract a large number of end members. Use of reference end members, in conjunction with image end members, might provide more impervious surface end members. In addition, multiple end member LSMA, instead of standard LSMA, may be applied for development of fraction images, if a large number of end members are desirable. This method has been applied to retrieve vegetation, soil, and snow cover, and has showed a better performance than the standard LSMA approach (Okin et al., 1999, 2001; Painter et al., 1998; Rashed et al., 2003; Roberts et al., 1998). The feasibility of applying a multiple end member LSMA approach to extract

Table 1
Definitions of urban land-use types

Urban land-use type	CODE	Definition
Low-intensity residential lands	LIRL	Impervious surface is very low, usually less than 30%; population density is less than 500 persons/km^2
Medium-intensity residential lands	MIRL	Impervious surface is usually greater than 20%, but often less than 50%; population density is between 500 and 1500 persons/km^2
High-intensity residential lands	HIRL	Impervious surface is usually greater than 40%; population density is between 1500 and 3000 persons/km^2
Very-high-intensity residential lands	VIRL	Impervious surface is usually greater than 50%; population density is greater than 3000 persons/km^2
Commercial, industrial, and transportation lands	CITL	Impervious surface is usually greater than 60%; population density is very low, usually less than 10 persons/km^2
Non-urban lands	NURL	Vegetated areas and agricultural lands
Water	WAT	Water bodies

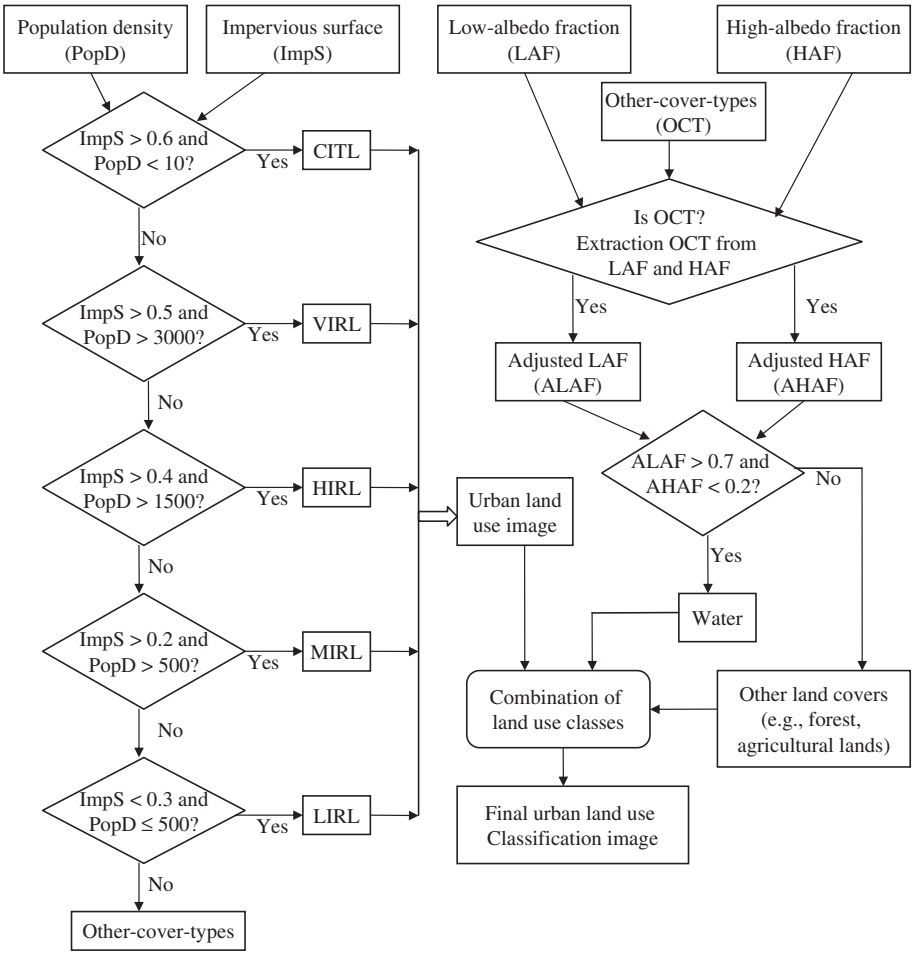

Fig. 10. Procedure for urban land-use classification based on the integration of impervious surface and population density images. ImpS and PopD represent impervious surface and population density (persons/km^2); and CITL, VIRL, HIRL, MIRL, and LIRL represent commercial/industrial/transportation lands, very-high-, high-, medium-, and low-intensity residential lands, respectively.

different impervious surface materials constitutes a promising direction for future research.

5.2. Issues related to urban land-use classification

Image classification is usually based directly on spectral signatures that are captured by remote sensors. However, complex landscapes with the mixed-pixel problem would lead to the difficulties in classification. In urban environments, classification algorithms based solely on spectral signatures cannot effectively handle the confusions (1) among water, dark impervious surface objects, and shadows from tall buildings or forest canopy; (2) among dry soils, commercial/industrial/transportation lands, and very high intensity residential lands; and (3) between forest and low-intensity residential lands. In particular, spectral-based classification approaches are not good at separating different densities of residential classes and not good at direct classification of urban land-use classes. Our research demonstrates that a classification approach based on the combination of impervious surface and population density can successfully solve these problems. Population data has not been extensively used for improvement of urban land-use classification in previous research. This may be due to the differences in data structures, spatial resolutions (scales), and coordinate systems between population data and remotely sensed data. The sizes of polygons for census units vary with urban land-use patterns. Hence, GIS plays an important role in the integration of population and remotely sensed data. This research indicates that setting up thresholds for impervious surface and population density for each urban land-use category is the key for success with this approach.

6. Conclusions

Five urban land-use classes can be successfully classified using medium spatial resolution remotely sensed data with an overall classification accuracy of 83.78%. The critical issue is to develop a high-quality impervious surface image. The integration of land surface temperature and LSMA-derived fraction images has been demonstrated to be effective for refining the impervious surface image, which has an overall RMSE of 9.22% and a system error of 5.68%. Because multispectral reflective images as well as thermal infrared images, such as Landsat TM/ETM+ and Terra ASTER, are readily available, estimation of impervious

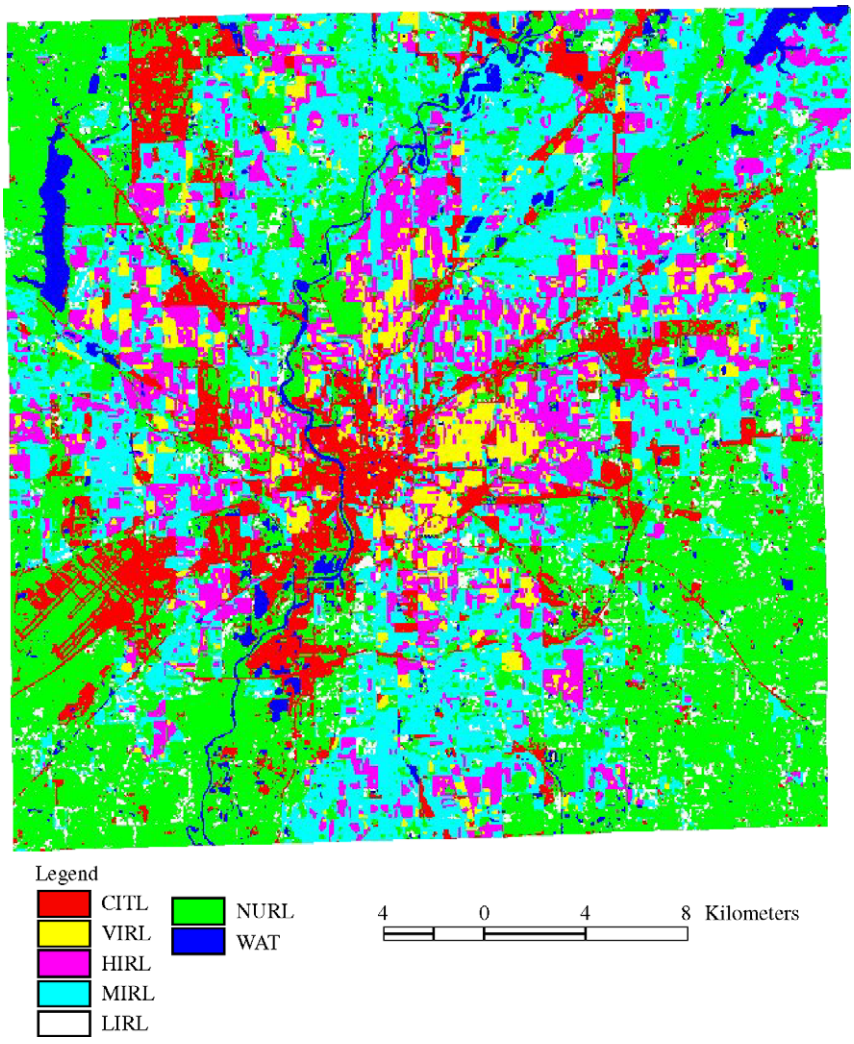

Fig. 11. Urban land-use classification image with the rule-based approach based on the integration of impervious surface and population density images. CITL, VIRL, HIRL, MIRL, and LIRL represent commercial/industrial/transportation lands, very-high-, high-, medium-, and low-intensity residential lands, respectively; NURL represents non-urban lands including vegetated and agricultural lands; and WAT represents water.

surface from remotely sensed data should be improved through the combinative use of land surface temperature and fraction images. The integration of impervious surface and population density provides a new insight for urban land-use classification and the approach developed in this paper can be applied to other urban environments.

Table 2
Accuracy assessment of the urban land-use classification image

	Reference data								
		LIRL	MIRL	HIRL	VIRL	CITL	NURL	WAT	RT	UA%
Classified data	LIRL	6					5		11	54.55
	MIRL	7	47	3					57	82.46
	HIRL		4	12					16	75.00
	VIRL			4	6				10	60.00
	CITL					22			22	100.00
	NURL	1	1			1	80		83	96.39
	WAT							7	7	100.00
	CT	14	52	19	6	23	85	7	206	
	PA%	42.86	90.38	63.16	100.00	95.65	94.12	100.00		87.38

(1) CITL, VIRL, HIRL, MIRL, and LIRL represent commercial/industrial/transportation lands, very-high-, high-, medium-, and low-intensity residential lands, respectively.
(2) NURL and WAT represent non-urban lands (vegetated and agricultural lands) and water.
(3) CT and RT mean column total and row total.
(4) PA and UA mean producer's accuracy and user's accuracy.
(5) The overall classification accuracies for seven classes and for five urban land-use classes are 87.38% and 83.78%.

Acknowledgments

The authors would like to thank three anonymous reviewers for their constructive comments and suggestions. This research is supported by National Science Foundation (BCS-0521734) for a project entitled "Role of Urban Canopy Composition and Structure in Determining Heat Islands: A Synthesis of Remote Sensing and Landscape Ecology Approach", and by the USGS IndianaView program and the NASA's Indiana Space Grant program for a project entitled "Indiana Impervious Surface Mapping Initiative." Dengsheng Lu also acknowledges the support from the Center for the Study of Institutions, Population, and Environmental Change at Indiana University, through the National Science Foundation (grants 99-06826).

References

Adams, J. B., Sabol, D. E., Kapos, V., Filho, R. A., Roberts, D. A., Smith, M. O., et al. (1995). Classification of multispectral images based on fractions of endmembers: Application to land cover change in the Brazilian Amazon. *Remote Sensing of Environment*, *52*, 137–154.

Aguiar, A. P. D., Shimabukuro, Y. E., & Mascarenhas, N. D. A. (1999). Use of synthetic bands derived from mixture models in the multispectral classification of remote sensing images. *International Journal of Remote Sensing*, *20*, 647–657.

Bauer, M. E., Heinert, N. J., Doyle, J. K., & Yuan, F. (2004). Impervious surface mapping and change monitoring using Landsat remote sensing. *ASPRS annual conference proceedings, May 23–28, 2004, Denver, Colorado.* Bethesda, MD: American Society for Photogrammetry and Remote Sensing.

Boardman, J. W., & Kruse, F. A. (1994). Automated spectral analysis: A geological example using AVIRIS data, north Grapevine Mountains, Nevada. *Proceedings, ERIM tenth thematic conference on geologic remote sensing, Ann Arbor, MI* (pp. 407–418).

Brabec, E., Schulte, S., & Richards, P. L. (2002). Impervious surface and water quality: A review of current literature and its implications for watershed planning. *Journal of Planning Literature*, *16*, 499–514.

Civico, D. L., Hurd, J. D., Wilson, E. H., Arnold, C. L., & Prisloe Jr., M. P. (2002). Quantifying and describing urbanizing landscapes in the northeast United States. *Photogrammetric Engineering and Remote Sensing*, *68*, 1083–1090.

Cochrane, M. A., & Souza Jr., C. M. (1998). Linear mixture model classification of burned forests in the eastern Amazon. *International Journal of Remote Sensing*, *19*, 3433–3440.

Congalton, R. G. (1991). A review of assessing the accuracy of classifications of remotely sensed data. *Remote Sensing of Environment*, *37*, 35–46.

Congalton, R. G., & Green, K. (1999). *Assessing the accuracy of remotely sensed data: Principles and practices.* Boca Raton, FL: CRC/Lewis Press.

Cracknell, A. P. (1998). Synergy in remote sensing – What's in a pixel? *International Journal of Remote Sensing*, *19*, 2025–2047.

Dare, P. M. (2005). Shadow analysis in high-resolution satellite imagery of urban areas. *Photogrammetric Engineering and Remote Sensing*, *71*, 169–177.

DeFries, R. S., Hansen, M. C., & Townshend, J. R. G. (2000). Global continuous fields of vegetation characteristics: A linear mixture model applied to multi-year 8 km AVHRR data. *International Journal of Remote Sensing*, *21*, 1389–1414.

Dougherty, M., Dymond, R. L., Goetz, S. J., Jantz, C. A., & Goulet, N. (2004). Evaluation of impervious surface estimates in a rapidly urbanizing watershed. *Photogrammetric Engineering and Remote Sensing*, *70*, 1275–1284.

ENVI. (2000). *ENVI user's guide.* Boulder, CA: Research Systems Inc.

Epstein, J., Payne, K., & Kramer, E. (2002). Techniques for mapping suburban sprawl. *Photogrammetric Engineering and Remote Sensing*, *63*, 913–918.

Fisher, P. (1997). The pixel: A snare and a delusion. *International Journal of Remote Sensing*, *18*, 679–685.

Foody, G. M. (2002). Status of land cover classification accuracy assessment. *Remote Sensing of Environment*, *80*, 185–201.

Garcia-Haro, F. J., Gilabert, M. A., & Melia, J. (1996). Linear spectral mixture modeling to estimate vegetation amount from optical spectral data. *International Journal of Remote Sensing*, *17*, 3373–3400.

Gillies, R. R., Box, J. B., Symanzik, J., & Rodemaker, E. J. (2003). Effects of urbanization on the aquatic fauna of the Line Creek watershed, Atlanta – a satellite perspective. *Remote Sensing of Environment*, *86*, 411–422.

Gluch, R. (2002). Urban growth detection using texture analysis on merged Landsat TM and SPOT-P data. *Photogrammetric Engineering and Remote Sensing*, *68*, 1283–1288.

Goetz, S. J., Jantz, C. A., Prince, S. D., Smith, A. J., Wright, R., & Varlyguin, D. (2004). Integrated analysis of ecosystem interactions with land use change: The Chesapeake Bay watershed. In R. S. DeFries, G. P. Asner, & R. A. Houghton (Eds.), *Ecosystems and land use change* (pp. 263–275). Washington, DC: American Geophysical Union.

Goetz, S. J., Wright, R., Smith, A. J., Zinecker, E., & Schaub, E. (2003). Ikonos imagery for resource management: Tree cover, impervious surface, and riparian buffer analyses in the mid-Atlantic region. *Remote Sensing of Environment*, *88*, 195–208.

Gong, P., & Howarth, P. J. (1990). The use of structure information for improving land-cover classification accuracies at the rural–urban fringe. *Photogrammetric Engineering and Remote Sensing*, *56*, 67–73.

Green, A. A., Berman, M., Switzer, P., & Craig, M. D. (1988). A transformation for ordering multispectral data in terms of image quality with implications for noise removal. *IEEE Transactions on Geoscience and Remote Sensing*, *26*, 65–74.

Haack, B. N., Solomon, E. K., Bechdol, M. A., & Herold, N. D. (2002). Radar and optical data comparison/integration for urban delineation: A case study. *Photogrammetric Engineering and Remote Sensing*, *68*, 1289–1296.

Harris, P. M., & Ventura, S. J. (1995). The integration of geographic data with remotely sensed imagery to improve classification in an urban area. *Photogrammetric Engineering and Remote Sensing*, *61*, 993–998.

Hodgson, M. E., Jensen, J. R., Tullis, J. A., Riordan, K. D., & Archer, C. M. (2003). Synergistic use of LiDAR ad color aerial photography for mapping urban parcel imperviousness. *Photogrammetric Engineering and Remote Sensing*, *69*, 973–980.

Hung, M., & Ridd, M. K. (2002). A subpixel classifier for urban land-cover mapping based on a maximum-likelihood approach and expert system rules. *Photogrammetric Engineering and Remote Sensing*, *68*, 1173–1180.

Jantz, P., Goetz, S. J., & Jantz, C. A. (2005). Urbanization and the loss of resource lands within the Chesapeake Bay watershed. *Environmental Management*, *36*, 808–825.

Jennings, D. B., Jarnagin, S. T., & Ebert, C. W. (2004). A modeling approach for estimating watershed impervious surface area from national land cover data 92. *Photogrammetric Engineering and Remote Sensing*, *70*, 1295–1307.

Ji, M., & Jensen, J. R. (1999). Effectiveness of subpixel analysis in detecting and quantifying urban imperviousness from Landsat Thematic Mapper. *Geocarto International*, *14*, 31–39.

Lu, D., Batistella, M., Moran, E., & Mausel, P. (2004). Application of spectral mixture analysis to Amazonian land-use and land-cover classification. *International Journal of Remote Sensing*, *25*, 5345–5358.

Lu, D., Moran, E., & Batistella, M. (2003). Linear mixture model applied to Amazonian vegetation classification. *Remote Sensing of Environment*, *87*, 456–469.

Lu, D., & Weng, Q. (2004). Spectral mixture analysis of the urban landscapes in Indianapolis with Landsat ETM+ imagery. *Photogrammetric Engineering and Remote Sensing*, *70*, 1053–1062.

Lu, D., & Weng, Q. (2005). Urban classification using full spectral information of Landsat ETM+ imagery in Marion County, Indiana. *Photogrammetric Engineering and Remote Sensing*, *71*, 1275–1284.

Mesev, V. (1998). The use of census data in urban image classification. *Photogrammetric Engineering and Remote Sensing*, *64*, 431–438.

Mustard, J. F., & Sunshine, J. M. (1999). Spectral analysis for earth science: Investigations using remote sensing data. In A. N. Rencz (Ed.), *Remote*

sensing for the earth sciences: Manual of remote sensing, *vol. 3* (3rd ed.) (pp. 251–307). New York, NY: John Wiley & Sons Inc.

Myint, S. W. (2001). A robust texture analysis and classification approach for urban land-use and land-cover feature discrimination. *Geocarto International*, *16*, 27–38.

Okin, W. J., Okin, G. S., Roberts, D. A., & Murray, B. (1999). Multiple endmember spectral mixture analysis: Endmember choice in an arid shrubland. In R. O. Green (Ed.), *The 1999 AVIRIS workshop.* Pasadena, CA: Jet Propulsion Laboratory.

Okin, G. S., Roberts, D. A., Murray, B., & Okin, W. J. (2001). Practical limits on hyperspectral vegetation discrimination in arid and semiarid environments. *Remote Sensing of Environment*, *77*, 212–225.

Painter, T. H., Roberts, D. A., Green, R. O., & Dozier, J. (1998). The effects of grain size on spectral mixture analysis of snow-covered area from AVIRIS data. *Remote Sensing of Environment*, *65*, 320–332.

Phinn, S., Stanford, M., Scarth, P., Murray, A. T., & Shyy, P. T. (2002). Monitoring the composition of urban environments based on the vegetation–impervious surface–soil (VIS) model by subpixel analysis techniques. *International Journal of Remote Sensing*, *23*, 4131–4153.

Rashed, T., Weeks, J. R., Gadalla, M. S., & Hill, A. G. (2001). Revealing the anatomy of cities through spectral mixture analysis of multispectral satellite imagery: A case study of the Greater Cairo region, Egypt. *Geocarto International*, *16*, 5–15.

Rashed, T., Weeks, J. R., Roberts, D., Rogan, J., & Powell, R. (2003). Measuring the physical composition of urban morphology using multiple endmember spectral mixture models. *Photogrammetric Engineering and Remote Sensing*, *69*, 1011–1020.

Ridd, M. K. (1995). Exploring a V–I–S (Vegetation–Impervious Surface–Soil) model for urban ecosystem analysis through remote sensing: Comparative anatomy for cities. *International Journal of Remote Sensing*, *16*, 2165–2185.

Roberts, D. A., Gardner, M., Church, R., Ustin, S., Scheer, G., & Green, R. O. (1998). Mapping chaparral in the Santa Monica mountains using multiple endmember spectral mixture models. *Remote Sensing of Environment*, *65*, 267–279.

Schueler, T. R. (1994). The importance of imperviousness. *Watershed Protection Techniques*, *1*, 100–111.

Shaban, M. A., & Dikshit, O. (2001). Improvement of classification in urban areas by the use of textural features: The case study of Lucknow city, Uttar Pradesh. *International Journal of Remote Sensing*, *22*, 565–593.

Slonecker, E. T., Jennings, D., & Garofalo, D. (2001). Remote sensing of impervious surface: A review. *Remote Sensing Reviews*, *20*, 227–255.

Small, C. (2001). Estimation of urban vegetation abundance by spectral mixture analysis. *International Journal of Remote Sensing*, *22*, 1305–1334.

Small, C. (2002). Multitemporal analysis of urban reflectance. *Remote Sensing of Environment*, *81*, 427–442.

Small, C. (2004). The Landsat ETM+ spectral mixing space. *Remote Sensing of Environment*, *93*, 1–17.

Smith, M. O., Ustin, S. L., Adams, J. B., & Gillespie, A. R. (1990). Vegetation in deserts: I. A regional measure of abundance from multispectral images. *Remote Sensing of Environment*, *31*, 1–26.

Smits, P. C., Dellepiane, S. G., & Schowengerdt, R. A. (1999). Quality assessment of image classification algorithms for land-cover mapping: A review and a proposal for a cost-based approach. *International Journal of Remote Sensing*, *20*, 1461–1486.

Stefanov, W. L., Ramsey, M. S., & Christensen, P. R. (2001). Monitoring urban land cover change: An expert system approach to land cover classification of semiarid to arid urban centers. *Remote Sensing of Environment*, *77*, 173–185.

Stuckens, J., Coppin, P. R., & Bauer, M. E. (2000). Integrating contextual information with per-pixel classification for improved land cover classification. *Remote Sensing of Environment*, *71*, 282–296.

Theseira, M. A., Thomas, G., Taylor, J. C., Gemmell, F., & Varjo, J. (2003). Sensitivity of mixture modeling to endmember selection. *International Journal of Remote Sensing*, *24*, 1559–1575.

Thomas, N., Hendrix, C., & Congalton, R. G. (2003). A comparison of urban mapping methods using high-resolution digital imagery. *Photogrammetric Engineering and Remote Sensing*, *69*, 963–972.

Van der Meer, F., & de Jong, S. M. (2000). Improving the results of spectral unmixing of Landsat Thematic Mapper imagery by enhancing the orthogonality of end-members. *International Journal of Remote Sensing*, *21*, 2781–2797.

Van der Sande, C. J., de Jong, S. M., & de Roo, A. P. J. (2003). A segmentation and classification approach of IKONOS-2 imagery for land cover mapping to assist flood risk and flood damage assessment. *International Journal of Applied Earth Observation and Geoinformation*, *4*, 217–229.

Weng, Q., Lu, D., & Schubring, J. (2004). Estimation of land surface temperature–vegetation abundance relationship for urban heat island studies. *Remote Sensing of Environment*, *89*, 467–483.

Wu, C. (2004). Normalized spectral mixture analysis for monitoring urban composition using ETM+ imagery. *Remote Sensing of Environment*, *93*, 480–492.

Wu, C., & Murray, A. T. (2003). Estimating impervious surface distribution by spectral mixture analysis. *Remote Sensing of Environment*, *84*, 493–505.

Yang, L., Huang, C., Homer, C. G., Wylie, B. K., & Coan, M. J. (2003). An approach for mapping large-area impervious surfaces: Synergistic use of Landsat-7 ETM+ and high spatial resolution imagery. *Canadian Journal of Remote Sensing*, *29*, 230–240.

Yang, L., Xian, G., Klaver, J. M., & Deal, B. (2003). Urban land cover change detection through sub-pixel imperviousness mapping using remotely sensed data. *Photogrammetric Engineering and Remote Sensing*, *69*, 1003–1010.

Zha, Y., Gao, J., & Ni, S. (2003). Use of normalized difference built-up index in automatically mapping urban areas from TM imagery. *International Journal of Remote Sensing*, *24*, 583–594.

Zhang, J., & Foody, G. M. (2001). Fully-fuzzy supervised classification of sub-urban land cover from remotely sensed imagery: Statistical neural network approaches. *International Journal of Remote Sensing*, *22*, 615–628.

Zhang, Q., & Wang, J. (2003). A rule-based urban land use inferring method for fine-resolution multispectral imagery. *Canadian Journal of Remote Sensing*, *29*, 1–13.